Atmospheric Turbulence Degraded Image Restoration by Kurtosis Minimization

Dalong Li, Steve Simske

HP Laboratories
HPL-2008-214

Keyword(s):
blur identification, atmospheric turbulence, image restoration, kurtosis.

Abstract:
Atmospheric turbulence is caused by the random fluctuations of the refraction index of the medium. It can lead to blurring in images acquired from a long distance away. Since the degradation is often not completely known, the problem is viewed as blind image deconvolution or blur identification. Our previous work has observed that blurring increases kurtosis and introduced a new blur identification method based on kurtosis minimization. In this letter, this observation has been studied using phase correlation. The kurtosis minimization method is compared with two other signal processing methods. The limitation of the method is also discussed.

External Posting Date: December 18, 2008 [Fulltext] Approved for External Publication
Internal Posting Date: December 18, 2008 [Fulltext]

To be published in IEEE Geoscience and Remote Sensing Letters.

Atmospheric Turbulence Degraded Image Restoration by Kurtosis Minimization

Dalong Li and Steven Simske, *Senior Member, IEEE*

***Abstract*— Atmospheric turbulence is caused by the random fluctuations of the refraction index of the medium. It can lead to blurring in images acquired from a long distance away. Since the degradation is often not completely known, the problem is viewed as blind image deconvolution or blur identification. Our previous work has observed that blurring increases kurtosis and introduced a new blur identification method based on kurtosis minimization. In this letter, this observation has been studied using phase correlation. The kurtosis minimization method is compared with two other signal processing methods. The limitation of the method is also discussed.**

***Index Terms*— blur identification, atmospheric turbulence, image restoration, kurtosis.**

I. Introduction

Random fluctuations of the refraction index cause atmospheric turbulence degradation. These phenomena have been observed in long-distance surveillance imagery and astronomy. The fluctuations in atmospheric turbulence can be modeled as a dynamic random process that perturbs the phase of the incoming light. The restoration of atmospheric turbulence degraded images has been actively studied [1]. From the refraction index structure functions, Hufnagel and Stanley [2] derived a long-exposure optical transfer function (OTF)

$$H(u,v) = e^{-\lambda(u^2+v^2)^{5/6}} \tag{1}$$

to model the long-term effect of turbulence in optical imaging. Here u and v are the horizontal and vertical frequency variables and λ parameterizes the severity of the blur. The refraction index fluctuation is a random process and the blurring parameter λ is dependent on many factors and in practise it is unknown. In such situations, it is formulated as a blur identification problem since the functional form of the blur is known but the parameter is not given. Besides blur identification methods, blind image deconvolution does not assume an atmospheric turbulence OTF [3], [4].

Blur identification methods often use parametric models. One of them is the Auto-Regressive Moving Average (ARMA) model, where the image is modeled as an autoregressive process and the blur is modeled as a moving average process. Maximum likelihood (ML) [5] and generalized cross-validation (GCV) [6] are two well-known examples that use this ARMA formulation. The ML algorithm estimates the image so that the likelihood of obtaining the observed image given the parameter is maximized. GCV identifies the parameter by minimizing a weighted sum of predictive errors. Restoration algorithms based on the ARMA model might converge to a local maximum when the parameter is high-dimensional. The two algorithms have been compared in [6] and the comparative studies favor GCV on real degraded images. In this letter, GCV based blur identification is compared with the proposed method.

Recently, Caron [4] introduced the Self-deconvolving Data Re-construction Algorithm (SeDDaRA), a blind image deconvolution method that first estimates OTF directly from the degraded image in the frequency domain and then uses Wiener filter to restore it. For comparison, the restoration results using SeDDaRA are also provided.

Based on an observed statistics, we had briefly reported the kurtosis minimization (KM) based blur identification method in [7]. In this letter, we analyze this observed statistics by phase correlation and compare with other blind image deconvolution algorithms. The limitation of the method and a possible solution is also discussed. This letter is organized as follow. Section II, the relationship between blurring and kurtosis is interpreted by phase correlation. KM based blur identification algorithm is briefly reviewed in section III. In section IV, the implementations, the comparative results and limitation of the method are reported. Some concluding remarks are in section V.

II. Kurtosis and smoothing

The kurtosis of a random variable is defined as the normalized fourth central moment

$$k = \frac{E((x-\mu)^4)}{\sigma^4} \tag{2}$$

where μ is the mean of x, σ is its standard deviation, and $E(x)$ represents the expectation of the variable. Previous research has noticed the non-Gaussian statistics of natural images. Particularly, it is shown that the histograms of filtered images tend to have single modes with heavy tails, characteristic of leptokurtic distributions. These statistics have been observed for derivative filters, Gabor filters, wavelets and even small random kernel filters [8]. Gluckman [9] used the phase structure to interpret the observed statistical regularities. Correlations in the phase angle of an image are used to explain the non-Gaussian statistics of natural images. Here we use the phase structures to analysis how blurring changes kurtosis.

A bandlimited signal $f(x)$ can be represented using a finite Fourier series

$$f(x) = \sum_{i=1}^{n} m_i cos(u_i x + \phi_i), \tag{3}$$

Manuscript received x XX, 2008; revised XX X, 2008.

Dalong Li is with Pegasus Imaging Corporation, Tampa, FL 33603 (e-mail: dalongli@gmail.com). Steven Simske is with the Print Production Automation Laboratory, Hewlett-Packard Laboratories, Fort Collins, CO 80528.

where m_i and ϕ_i are the magnitude and phase angle associated with integer frequency u_i. For simplicity, we consider the 1D case and assume $f(x)$ is zero-mean. Since a symmetric image can always be created by reflection, the Fourier transform of the signal is real. Thus, the phase of each frequency is either 0 or π, and is represented by the signed magnitudes $s_i \in \{-1, 1\}$. The signal can be represented as a sum of low-frequency components $f_l(x)$ and high-frequency components $f_h(x)$. $f_l(x)$ and $f_h(x)$ are abbreviated as f_l and f_h in some of the following equations.

$$f_l(x) = \sum_{i=1}^{n} m_{l,i} cos(u_{l,i}x + \phi_{l,i}) \tag{4}$$

$$f_h(x) = \sum_{i=1}^{m} m_{h,i} cos(u_{h,i}x + \phi_{h,i}) \tag{5}$$

The k^{th} central moment of f is:

$$\mu_k(f) = \frac{1}{|\Omega|}\int_\Omega f^k(x) d\Omega \tag{6}$$

where Ω is the image domain.

The 4^{th} order moment of f is

$$\begin{aligned} \mu_4(f(x)) &= \mu_4(f_l(x) + f_h(x)) \\ &= \frac{1}{|\Omega|}\int_\Omega (f_l(x) + f_h(x))^4 d\Omega \\ &= \mu_{40} + 4\mu_{31} + 6\mu_{22} + 4\mu_{13} + \mu_{04} \end{aligned} \tag{7}$$

$$\begin{aligned} \mu_{31} &= \frac{3}{4}\sum_{i,j,r,v}\{(m_{l,i}m_{l,j}m_{l,r}m_{h,v})(s_{l,i}s_{l,j}s_{l,r}s_{h,v}) \\ &\quad I(i,j,r,v)\} \\ \mu_{13} &= \frac{3}{4}\sum_{i,j,r,v}\{(m_{l,i}m_{h,j}m_{h,r}m_{h,v})(s_{l,i}s_{h,j}s_{h,r}s_{h,v}) \\ &\quad I(i,j,r,v)\} \\ \mu_{22} &= \mu_{20}\mu_{02} \\ &+ \frac{1}{2}\sum_{i,j,r,v}\{(m_{l,i}m_{l,j}m_{h,r}m_{h,v})(s_{l,i}s_{l,j}s_{h,r}s_{h,v}) \\ &\quad I(i,j,r,v)\} \end{aligned}$$

where $I(i,j,r,v)$ is an indicator function[9]

$$I(i,j,r,v) = \begin{cases} 1 & \textit{if } (u_i - u_j) = (u_r - u_v) \\ 0 & \textit{otherwise} \end{cases} \tag{8}$$

The moments $\mu_{13} \approx 0$ and $\mu_{31} \approx 0$ because $(u_i - u_j) = (u_r - u_v)$ usually does not hold when 3 of the four frequencies $\{i, j, r, v\}$ are in a single band (low or high).

The kurtosis of $f(x)$ is then

$$\begin{aligned} k_f &= \frac{\mu_4(f)}{\mu_2^2(f)} \\ &= \frac{\mu_{40}(f_l) + \mu_{40}(f_h) + 6(\mu_{20}(f_l)\mu_{02}(f_h)) + 3C}{(\mu_{20}(f_l) + \mu_{20}(f_h))^2} \end{aligned} \tag{9}$$

where $C = \sum_{i,j,r,v}\{(m_{l,i}m_{l,j}m_{h,r}m_{h,v})(s_{l,i}s_{l,j}s_{h,r}s_{h,v})$ $I(i,j,r,v)$ and $\mu_{20}(f_h)$ refers to the μ_{20} of the high frequency component, other μ follows the same manner. The kurtosis of $f_l(x)$ and $f_h(x)$ are:

$$\begin{aligned} k_{f_l} &= \frac{\mu_{40}(f_l)}{\mu_{20}^2(f_l)} \\ k_{f_h} &= \frac{\mu_{40}(f_h)}{\mu_{20}^2(f_h)} \end{aligned} \tag{10}$$

From Eq. (9) and Eq. (10), the condition for $k_{f_l} > k_f$ is

$$3C < \mu_{20}(f_l)\mu_{20}(f_h)(2k_{f_l} - 6) + (k_{f_l} - k_{f_h})\mu_{20}^2(f_h) \tag{11}$$

A blurring PSF is a low pass filter. Therefore, for some natural images, blurring will increase kurtosis. The smoothed (blurred) image has higher kurtosis than the original image. In general, this is not true for binary image.

III. Kurtosis minimization for blur identification

Given a noisy blurred image g with a known functional form for the blur, we estimate the blur parameter λ. The search space Ω is set manually on a trial-and-error basis. If the upper limit of λ is too large, then the corresponding restored image would be very degraded.

At each step in the search loop, the image is deblurred using a Wiener filter $G(u, v)$ or any other non-blind restoration algorithm and the kurtosis of the deblurred image $\hat{f}(\lambda)$ is computed and recorded. Then the deblurred image with the minimal kurtosis is chosen as the final restored image and the corresponding parameter is regarded as the identified blurring parameter. The kurtosis minimization based blur identification can be summarized as

$$\lambda_k = \arg\{\min_{\lambda\in\Omega} k(\hat{f}(\lambda))\}. \tag{12}$$

The non-blind restoration algorithm used in this work is the practical form of the Wiener filter:

$$G(u, v) = \frac{H^*(u, v)}{|H(u, v)|^2 + nsr} \tag{13}$$

where nsr is the noise to signal ratio. Since the signal is unknown, in practice, the noise-to-signal ratio is approximated by the noise-to-blurred-signal ratio, which can be estimated either in the spatial domain or in the frequency domain.The Wiener filter behaves as a mid-band emphasis filter. In the region where signal is very strong relative to the noise, $P_n(u, v)/P_f(u, v) \approx 0$ and the Wiener filter approximates $H^{-1}(u, v)$ (the inverse filter). In the region where signal is very weak, $P_n(u, v)/P_f(u, v) \to \infty$ and $G(u, v) \to 0$ to prevent noise amplification. Such characteristics of the Wiener filter are critical to the kurtosis minimization based blur identification. If noise is amplified in the restoration, for example, by an inverse filter, the kurtosis of the corresponding restored image will be low and the kurtosis minimization will not find the correct restored image. In that case, kurtosis minimization might fail because the non-blind restoration algorithm does not provide a reasonable candidate.

TABLE I
PSNR (DB) COMPARISONS OF THE THREE IMAGE RESTORATION METHODS.

Image	degraded	KM	GCV	SeDDaRA
aerial	20.33	**21.12**	21.05	19.94
tree	20.62	**22.91**	22.11	16.36
peppers	25.54	26.51	**26.62**	18.87
boat	22.67	**23.97**	23.35	20.02
Lena	24.68	**25.72**	25.01	22.13

IV. EXPERIMENTS ON REAL AND SIMULATED ATMOSPHERIC TURBULENCE BLURRED IMAGES

Example on a real atmospheric turbulence degraded image is shown here. For both GCV and KM, the parameter search space $\Omega_\lambda = \{\lambda : 0.0004i | i = 0, 1, 2, \dots, 25\}$. The upper limit is set by trial and error. In SeDDaRA, the tuning parameter α is set as 0.4. Fig. 1 shows the results. The λ identified by GCV is 0.0004. The image appears to be "under-deblured". KM identified it as 0.0012. High frequency components are amplified and the image is effectively "sharpened". The SeDDaRA result appears to be "over-deblurred" and the image looks unnatural. However, in terms of complexity, among the three, SeDDaRA has the lowest complexity as it is non-iterative in nature. The size of the image is 240 by 240, on a 1.4GHz Intel Pentium laptop computer with 768 MB of RAM, it took 0.55 seconds to restore the image. Both GCV and KM have higher complexity. GCV took 11.76 seconds and KM took 8.98 seconds.

Several test images were selected from the USC-SIPI image database [10] for the experiments of restoring the simulated atmospheric turbulence blur. Since the ground-truth images are available, the Peak signal-to-noise ratio (PSNR) can be used to measure the quality of the restored images. PSNR is defined as:

$$PSNR = 10 \log_{10} \frac{\sum_{i=1}^{M} \sum_{j=1}^{N} 255^2}{\sum_{i=1}^{M} \sum_{j=1}^{N} (f(i,j) - \hat{f}(i,j))^2} \quad (14)$$

where $\hat{f}(i,j)$ is the restored image, and $f(i,j)$ is the ground-truth image. The size of the images are $M \times N$. In the simulation experiments, the ground-truth images were blurred with the Hufnagel and Stanley model ($\lambda = 0.004$) and Gaussian random noise ($\sigma^2 = 0.001$) was added to the blurred images. Table I shows the results of the comparisons. KM has slightly lower PSNR on the PEPPERS image. For all other images, KM results are the best. The SeDDaRA results have the lowest PSNR since the method is not robust to noise and the parameter α might need to be chosen manually.

If the parameter space is estimated properly, the kurtosis profile is expected to be concave. Since KM is built upon an observed statistics of images (blurred image has higher kurtosis), it is possible for some images not to follow the statistics. One possible way to overcome the limitation is to subdivide the image into overlapped sub-images. The statistics of sub-images are different from the whole image. From the sub-images that follow the kurtosis statistics, the parameter can be estimated. To identify such sub-image, we can first blur it with the Hufnagel and Stanley model (λ can be set as 0.004) and then compute its kurtosis and compare with the kurtosis of the sub-image before the blurring. If the kurtosis increases, then the sub-image is believed to be proper for the kurtosis minimization based blur identification. In case there are more than one such sub-images, the identified λs are averaged to give the over-all estimation. An example is shown in Fig. 2. The image is blurred by atmospheric turbulence blur at $\lambda = 0.01$. Then Gaussian noise is added at $\sigma^2 = 0.0006$. Though the kurtosis profile of the entire image is not concave, that of the sub-image is concave and the minimum is located very close to the true blurring λ.

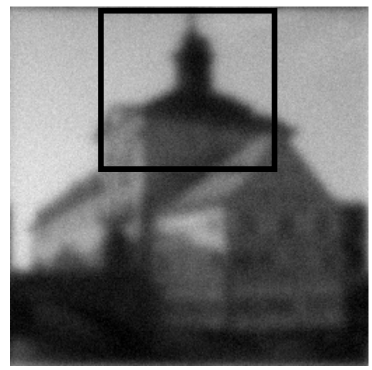

(a) A simulated blurred image.

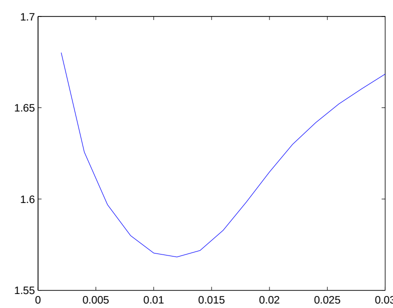

(b) The kurtosis profile as a function of λ.

Fig. 2. Example of the sub-image approach.

V. CONCLUSION

We furthered the kurtosis minimization based blur identification work. The observed kurtosis statistics is analysized theoretically in frequency domain by phase correlation. Its application in restoring image degraded by atmospheric turbulence is highlighted in this letter. The restoration of such image is viewed as a blind deconvolution or a blur identification problem in image processing. Since blur identification methods use a model for the OTF, they tend to achieve better results than blind deconvolution methods which do not consider the functional form of OTF. Comparisons with other methods suggest that KM is competitive in restoring images degraded by atmospheric turbulence blur. KM is built upon statistics and there is no guarantee that it will work on any given image. Sub-image approach is an attempt to overcome this limitation.

(a) The blurred image.

(b) The restored image with kurtosis minimization identified $\lambda = 0.0012$.

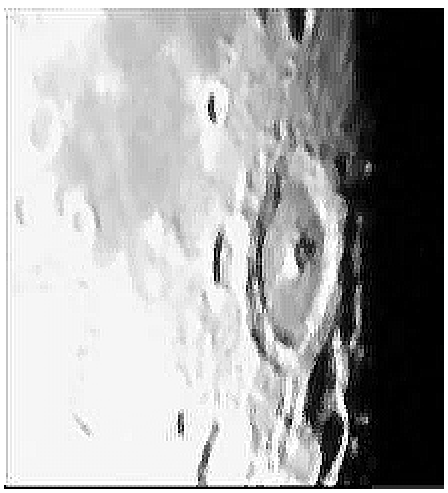

(c) The restored image with kurtosis minimization identified $\lambda = 0.0004$.

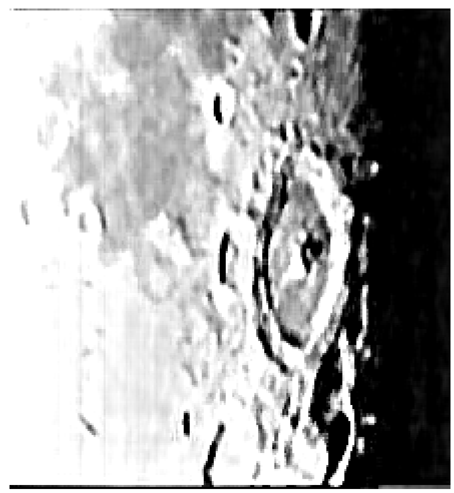

(d) The image restored by the SeDDaRA ($\alpha = 0.4$).

Fig. 1. Comparative results on a real turbulence degraded image.

REFERENCES

[1] B. L. Ellerbroke and T. A. Rhoadarmer, "Adaptive wavefront control algorithms for closed loop adaptive optics," *Math. Comput. Model*, vol. 33, pp. 145–158, 2001.

[2] R. E. Hufnagel and N. R. Stanley, "Modulation Transfer Function Associated with Image Transmission through Turbulence Media," *Optical Society of America Journal A*, vol. 54, pp. 52–61, 1964.

[3] D. Li, R. M. Mersereau, and S. Simske, "Atmospheric turbulence-degraded image restoration using principal components analysis.," *IEEE Geoscience and Remote Sensing Letters*, vol. 4, no. 3, pp. 340–344, 2007.

[4] J. N. Caron, N. M. Namazi, and C. J. Rollins, "Noniterative blind data restoration by use of an extracted filter function.," *Appl. Opt.*, vol. 41, no. 32, pp. 6884–6889, 2002.

[5] J. Biemond, A. M. Tekalp, and R. L. Lagendijk, "Maximum likelihood image and blur identification: a unifying approach," *Optical Engineering*, vol. 29, pp. 422–435, May 1990.

[6] S.J. Reeves and R.M. Mersereau, "Blur Identification by the Method of Generalized Cross-validation," *IEEE Trans Image Processing*, vol. 1, no. 3, pp. 301–311, July 1992.

[7] D. Li, R. M. Mersereau, and S. Simske, "Blur identification based on kurtosis minimization," in *Proc. IEEE ICIP '2005*, Genoa,Italy, 2005, vol. 1, pp. 905–908.

[8] A. Srivastava, A. B. Lee, E. P. Simoncelli, and S. C. Zhu, "On advances in statistical modeling of natural images," *Journal of Mathematical Imaging and Vision*, vol. 18, no. 1, Jan. 2003.

[9] G. M. Gluckman, "Kurtosis and the Phase Structure of Images," in *3rd International Workshop on Statistical and Computational Theories of Vision, Nice, France, October 2003 (in conjunction with ICCV '03)*, Nice, France, 12–15, 2003.

[10] *University of Southern California - Signal & Image Processing Institute - The USC-SIPI Image Database*, http://sipi.usc.edu/services/database/Database.html.